

Nanosize-Enhanced Lifetime of SAPO-34 Catalysts in Methanol-to-Olefin Reactions

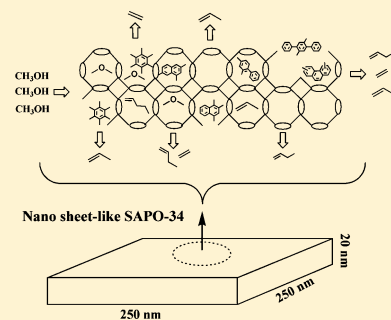
Guoju Yang,^{†,‡} Yingxu Wei,[†] Shutao Xu,[†] Jingrun Chen,[†] Jinzhe Li,[†] Zhongmin Liu,^{*,†} Jihong Yu,^{*,‡} and Ruren Xu[‡]

[†]National Engineering Laboratory for Methanol to Olefins, Dalian National Laboratory for Clean Energy, Dalian Institute of Chemical Physics, Chinese Academy of Sciences, Dalian 116023, P. R. China

[‡]State Key Laboratory of Inorganic Synthesis and Preparative Chemistry, College of Chemistry, Jilin University, Changchun 130012, P. R. China

S Supporting Information

ABSTRACT: In this work, we systematically investigated the size effect of silicoaluminophosphate molecular sieve catalysts SAPO-34 on the catalytic performance of methanol-to-olefin (MTO) reactions. Four highly crystalline SAPO-34 molecular sieves with different crystallite sizes were synthesized under hydrothermal conditions carried out in conventional or microwave ovens with the same starting gel composition using TEOAH as the structure-directing agent. The as-prepared SAPO-34s have similar composition, and their average crystal size can be controlled between 20 nm and 8 μm . Textural properties and chemical environments of framework atoms as well as acid concentration were characterized by N_2 adsorption and NMR measurements. The MTO reactions were carried out over these four SAPO-34 catalysts to study their catalytic performances dependent on the crystal size. The occurrence of catalyst deactivation varied considerably with the crystal size of SAPO-34s. Significantly, the nanosized catalysts, especially the sheetlike SAPO-34 catalyst with 20 nm thickness, exhibited the longest catalyst lifetime and lowest coking rate in MTO reactions. On the basis of the measurement of coke formation and the determination of retained coke species, a scheme is proposed to elucidate the reduction in coke deposition and consequently the remarkably enhanced lifetime on the nanosized SAPO-34 catalysts in methanol conversion.



1. INTRODUCTION

The rapid increase in the price of crude oil and its shortage in the foreseeable future make the alternative route for the production of some important petrochemical products, such as light olefins, more attractive than ever before.^{1,2} The methanol-to-olefin (MTO) process has proven to be the most successful nonpetrochemical route for the production of light olefins, such as ethylene and propylene, from the abundant resources of natural gas or coal.³ Aluminosilicate zeolite ZSM-5^{4–6} and silicoaluminophosphate molecular sieve SAPO-34^{7–9} are excellent catalysts for the MTO reactions. In comparison with ZSM-5, the selectivity toward light olefins is significantly improved by the application of SAPO-34 with CHA cage and eight-ring pore opening. Under an optimized reaction condition, selectivity to light olefins over SAPO-34 may exceed 90%.¹⁰ However, during methanol conversion, SAPO-34 catalyst with large cavities connected by narrow channels also accommodates a large amount of organic species as retained materials, which cause rapid catalyst deactivation. Fluidized-bed reaction with recycling reaction-regeneration technique has been applied in the industrial MTO process with SAPO-34 as the catalyst to maintain the reactivity of catalyst in the reactor.^{11,12} Some strategies have also been considered in depressing the coke generation, such as optimizing the operating conditions¹³ or modifying the zeolite pore structure

and acidity, to prolong the lifespan of the catalyst in MTO reactions. Previous studies revealed that deactivation of catalysts in catalytic reactions mainly stemmed from the restriction in mass transfer with coke deposition, while the catalysts with small crystallite size showed their advantage in the enhancement of mass transfer and the reduction in coke formation.^{14,15} As for the effect of SAPO-34 particle size on its performance in MTO reactions, in an early work reported by Chen and co-workers, the fractions of SAPO-34 molecular sieves with various crystallite sizes were separated, and their performance in MTO reactions exhibited the effects of crystal size on the product selectivity and coke deposition rate.¹⁶ Recently, Chen et al. emphasized that the use of SAPO-34 with small size in MTO reactions can achieve a low coke selectivity and low deactivation due to reduce of diffusion limitation.¹⁷ With the development of nanoscale molecular sieve synthesis, nanosized SAPO-34s¹⁸ were employed as the catalysts of methanol conversion, and improved methanol conversion efficiency and prolonged catalyst lifetime were exhibited, compared to the catalysts with ordinary crystal size.^{19–22} The short diffusion length in nanoscale catalyst, resulting in the

Received: December 30, 2012

Revised: March 18, 2013

Published: March 25, 2013

Table 1. Synthesis Conditions of SAPO-34s and Measurement Results of XRF and SEM

catalysts	Si source	synthesis conditions			XRF		SEM
		heating method	$T / ^\circ\text{C}$	time/h	molar composition	particle size/ μm	morphology
SP-S	colloidal silica	microwave-assisted	180	1	$\text{Si}_{0.12}\text{Al}_{0.48}\text{P}_{0.40}\text{O}_2$	$0.02 \times 0.25 \times 0.25$	flake
SP-F	TEOS	microwave-assisted	180	1	$\text{Si}_{0.11}\text{Al}_{0.48}\text{P}_{0.41}\text{O}_2$	0.08	nanosphere ^a
SP-M	Na_2SiO_3	microwave-assisted	200	2	$\text{Si}_{0.10}\text{Al}_{0.50}\text{P}_{0.40}\text{O}_2$	$1 \times 1 \times 1$	cube
SP-C	Na_2SiO_3	conventional method	200	72	$\text{Si}_{0.11}\text{Al}_{0.49}\text{P}_{0.40}\text{O}_2$	$8 \times 8 \times 8$	cube

^aSP-F is an 80 nm spherical aggregation of the smallest crystals of ca. 20 nm, as shown in the TEM image in Figure S1.

reduction of residence time of reactant and products of MTO reactions, was used to explain the long catalyst lifetime of nanocrystals.¹⁹ The increase in the accessible cages near external surface for the SAPO-34 nanoscale catalyst was proved very helpful in improving the conversion efficiency of the SAPO-34 catalyst in the methanol conversion.^{20,22} However, Jang et al. found that the smallest nanocrystallites of SAPO-34 (<150 nm) tested in their work had a detrimental effect on the catalyst lifetime due to the severe pore blockage by coke deposited on the external surfaces of the nanoparticles.²³

The SAPO-34 catalysts with different particle size distributions were obtained mainly through fractionation or synthesized with different structure-directing agents (SDAs) in the above-mentioned reports.^{16,19,20,23} In the present study, four highly crystalline SAPO-34 catalysts with different crystallite sizes (between 20 nm and 8 μm) were synthesized from the starting gel with the same composition under conventional hydrothermal and microwave-assisted heating conditions, using TEOH as the sole SDA. Methanol conversion was performed over the synthesized SAPO-34s to investigate the influence of crystallite size on the catalytic performance. The differences in the textural properties, chemical environments of framework atoms, and acid site distributions of the four catalysts were correlated to the catalyst lifetime and product selectivity. The deactivation behavior and mechanism over the four SAPO-34s with different crystal sizes were studied in combination with catalytic test and confined organics analysis. Our study clearly demonstrated the remarkably enhanced lifetime of nanosized SAPO-34 catalysts in MTO reactions. The catalytic performance dependent on the crystallite size has been elucidated. This work will provide useful guidance for the improvement of methanol conversion process by utilizing nano SAPO-34 catalysts.

2. EXPERIMENTAL SECTION

2.1. Synthesis. The reagents used were aluminum isopropoxide ($\text{Al}(\text{OPr}^i)_3$, 99.5 wt %, Beijing Reagents Company), phosphoric acid (H_3PO_4 , 85 wt %, Beijing Chemical Works), tetraethylammonium hydroxide solution (TEAOH, 35 wt %, Alfa Aesar), colloidal silica (30 wt %, Aldrich), tetraethylorthosilicate (TEOS, 28 wt % SiO_2 , Beijing Chemical Works), and sodium silicate solution (Na_2SiO_3 , 26.5 wt % SiO_2 , Changling Refining Company).

The SAPO-34 crystals with varied crystallite sizes were synthesized from the starting gel with the same molar composition of $1.0\text{Al}_2\text{O}_3 \cdot 2.0\text{P}_2\text{O}_5 \cdot 4.0\text{TEAOH} \cdot 0.6\text{SiO}_2 \cdot 140\text{H}_2\text{O}$. The nanosized SAPO-34 catalysts were prepared under microwave radiations following previously reported method by using colloidal silica or TEOS as the silicon source.²⁴ The SAPO-34 catalysts with medium and ordinary size were obtained with Na_2SiO_3 solution as the silicon source under hydrothermal or microwave-assisted conditions. Typi-

cally, the finely ground $\text{Al}(\text{OPr}^i)_3$ was first mixed with TEOH solution and deionized water at room temperature until dissolved completely. Na_2SiO_3 solution was then added, followed by continuous stirring for 4 h. Finally, phosphoric acid was added dropwise to the resultant solution. The reaction mixture was further stirred for 2 h prior to being transferred into a Teflon-lined autoclave. The crystallization was conducted in a microwave oven (Milestone ETHOS-D) with preprogrammed heating profiles at 200 $^\circ\text{C}$ for 2 h for the synthesis of SAPO-34 with medium size and in a conventional oven at 200 $^\circ\text{C}$ for 3 days under static conditions for the synthesis of SAPO-34 with coarse particles. The synthesis conditions are detailed in Table 1. According to the crystallite size and morphology, the synthesized SAPO-34 were named as SP-S, SP-F, SP-M, and SP-C, representing the sheetlike, fine, medium, and coarse particles. The as-synthesized solid products were centrifuged, washed with water and ethanol several times, and then dried at room temperature overnight, followed by calcination at 550 $^\circ\text{C}$ for 6 h.

2.2. Characterization. The crystallinity and phase purity of the samples were characterized by powder X-ray diffraction on a PANalyticalX'Pert PRO X-ray diffractometer with $\text{Cu K}\alpha$ radiation ($\lambda = 0.15418 \text{ nm}$). The crystal size and morphology were measured by scanning electron microscopy (SEM) using a JSM-6700F electron microscope operating at 5.0 KV and transmission electron microscopy (TEM) examined with a JEM-2100 TEM operated at 200 kV. Chemical composition was determined with an X-ray fluorescence (XRF) spectrometer (Philips Magix-601). Nitrogen adsorption–desorption measurement was carried out on a Micromeritics 2020 analyzer at 77.35 K after the sample was degassed at 350 $^\circ\text{C}$ under vacuum.

²⁹Si, ²⁷Al, ³¹P, and ¹H MAS NMR experiments were performed on a 600 MHz Bruker Avance III equipped with a 4 mm MAS probe. ²⁹Si MAS NMR spectra were recorded using high-power proton decoupling with a spinning rate of 10 kHz. A total of 1024 scans were accumulated with a $\pi/2$ pulse width of 3 μs and a 10 s recycle delay. The chemical shifts were referenced to DSS (4,4-dimethyl-4-silapentane sulfonate sodium) at 0 ppm. ²⁷Al MAS NMR spectra were recorded using a one-pulse sequence with a spinning rate of 12 kHz. One-hundred scans were accumulated with a $\pi/8$ pulse width of 0.75 μs and a 2 s recycle delay. The chemical shifts were referenced to $(\text{NH}_4)\text{Al}(\text{SO}_4)_2 \cdot 12\text{H}_2\text{O}$ at -0.4 ppm . ³¹P MAS NMR spectra were recorded using high-power proton decoupling with a spinning rate of 12 kHz. Forty-eight scans were accumulated with a $\pi/4$ pulse width of 2 μs and a 10 s recycle delay. The chemical shifts were referenced to 85% H_3PO_4 at 0 ppm.

¹H MAS NMR spectra were recorded using a 4 mm MAS probe. The pulse width was 2.2 μs for a $\pi/4$ pulse, and 32 scans were accumulated with a 4 s recycle delay. Samples were spun at 12 kHz, and chemical shifts were referenced to adamantane

at 1.74 ppm. The software Dmfit was employed for deconvolution using fitting of Gaussian–Lorentzian line shapes. Before ^1H MAS NMR measurements of adsorption of perfluorotributylamine (analytical standard, from Sigma-Aldrich) on SAPO-34 samples, the samples were dehydrated typically at 693 K under pressure below 10^{-3} Pa for 20 h before adsorption. Selective adsorption of perfluorotributylamine was performed by exposing the dehydrated sample to saturated vapor at room temperature for 30 min. After equilibration, the samples were degassed at 298 K to remove the physical adsorbate on the surface.

2.3. Catalytic Test and Retained Coke Analysis.

Methanol conversion was performed in a quartz tubular fixed-bed reactor at atmospheric pressure. The catalyst (100 mg) loaded in the quartz reactor was activated at 500 °C in a He flow of 30 mL/min for 1 h before starting each reaction run, and then the temperature was adjusted to a reaction temperature of 400 °C. The methanol was fed by passing the carrier gas (4.2 mL/min) through a saturator containing methanol at 33 °C, which gave a WHSV of 2.0 h^{-1} . The reaction products were analyzed using an online gas chromatograph (Agilent GC 7890N), equipped with a flame ionization detector (FID) and Plot-Q column. The conversion and selectivity were calculated on CH_2 basis. Dimethyl ether (DME) was considered as reactant in the calculation.

The amount of generated coke in SAPO-34 catalysts after the reactions of methanol was determined by thermal analysis (TG-DTA) on a TA Q600 analyzer at the temperature range of 50–800 °C with a heating rate of 10 °C/min under an air flow of 100 mL/min. The retained organics in the deactivated SAPO-34 catalysts with different particle sizes after the reaction of methanol were analyzed according to the procedure introduced by Guisnet.^{25,26} Typically, after dissolving the completely deactivated catalyst with a HF solution (20 wt %), the confined organic compounds of the deactivated catalysts were extracted in a CH_2Cl_2 solution and analyzed by a gas chromatograph equipped with a FID detector and a mass sensitive detector (Agilent 7890A/5975C) using a capillary column of HP-5.

3. RESULTS AND DISCUSSION

3.1. Crystallinity, Textural Properties and Morphology of Synthesized SAPO-34s with Varied Particle Sizes.

As shown in Figure 1, all the XRD patterns of as-synthesized SAPO-34s match well with that simulated from the CHA framework type. The intensities and the width of the Bragg reflections peaks vary with the crystal size. The diffraction peaks are sharp and intensified for the SAPO-34 with medium-sized and coarse particles (SP-M and SP-C), while for the nanoscale crystallites, they are relatively broad and weak. Figure 2 shows the SEM images. Except the nanosheet-like SAPO-34 (SP-S, $20 \times 250 \times 250$ nm) and the nanosphere SP-F (dia. ~ 80 nm, formed by aggregation of the smallest crystals of ca. 20 nm, as shown in Figure S1), both SP-M and SP-C exhibit a similar cubic morphology with the average crystallite sizes of 1 and 8 μm , respectively. It can be seen that microwave heating resulted in the formation of crystal particles in nanosize, much smaller than those synthesized by conventional heating.

The compositions of the prepared SAPO-34s, determined by XRF spectrometer, are shown in Table 1. The composition of SAPO-34 is expressed as $\text{Al}_x\text{P}_y\text{Si}_z\text{O}_2$, where x , y , z represent the mole fractions of aluminum, phosphorus, and silicon, respectively, with $x + y + z = 1$. The contents of Al, P, Si of all the samples are very close because of the same starting gel

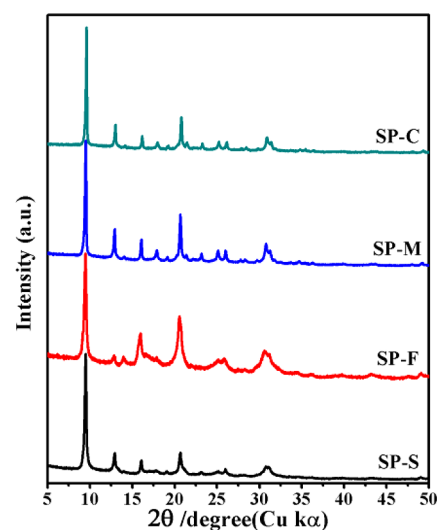


Figure 1. XRD patterns of synthesized SAPO-34s with different crystal particle sizes.

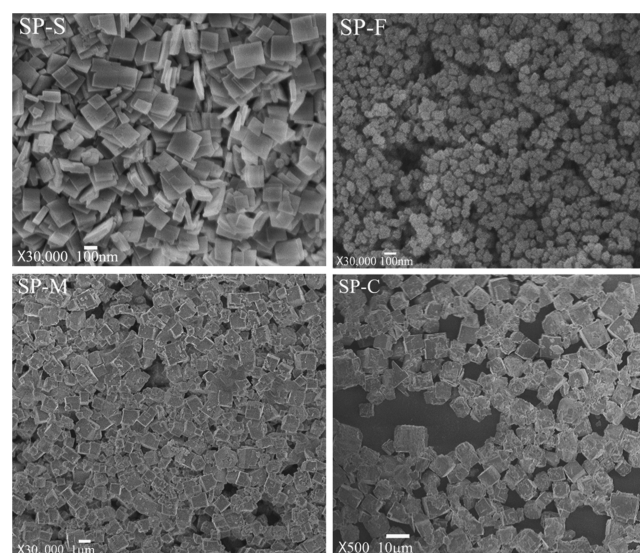


Figure 2. SEM images of synthesized SAPO-34s with different crystal particle sizes.

composition and the use of TEOH as the only SDA.²⁷ Very slight difference in composition implies that heating method, conventional or microwave-assisted method, i.e., which resulted in the difference in crystallite size, has no remarkable influence on the framework element composition.

The textural properties of calcined SAPO-34s were determined with nitrogen adsorption–desorption measurement and tabulated in Table 2. From the table, it can be summarized that the surface areas vary with the crystal sizes of the synthesized SAPO-34s. With the decrease of the particle size,

Table 2. Variation of Textural Properties of Synthesized SAPO-34s with Different Crystal Particle Sizes

catalysts	S_{total} (m^2/g)	S_{micro} (m^2/g)	S_{ext} (m^2/g)	V_{micro} (cm^3/g)
SP-S	599	508	91	0.24
SP-F	535	394	141	0.18
SP-M	433	408	25	0.19
SP-C	386	343	42	0.16

the surface area is greatly enhanced. Accordingly, SP-S with the smallest particle size has the largest surface area, while SP-C with the largest particle size presents the smallest surface area. It is notable that nanosized SAPO-34s possess more external surface than the SAPO-34s with ordinary size. The adsorption at the high relative pressure (Figure S2) indicates the existence of some mesoporous or macroporous surface in nanosized particles, contributing to the increase of surface area, especially the external surface area. Even with the difference in surface area, the four samples, regardless of their crystallite size, all exhibit micropore volume around $0.2 \text{ cm}^3/\text{g}$.

3.2. Chemical Environments of Framework Atoms and Acidity Measurements by Solid-State NMR. Solid-state ^{29}Si , ^{31}P , and ^{27}Al MAS NMR spectroscopies were employed to investigate the chemical environments of framework atoms. ^{27}Al MAS NMR spectra in Figure 3a present

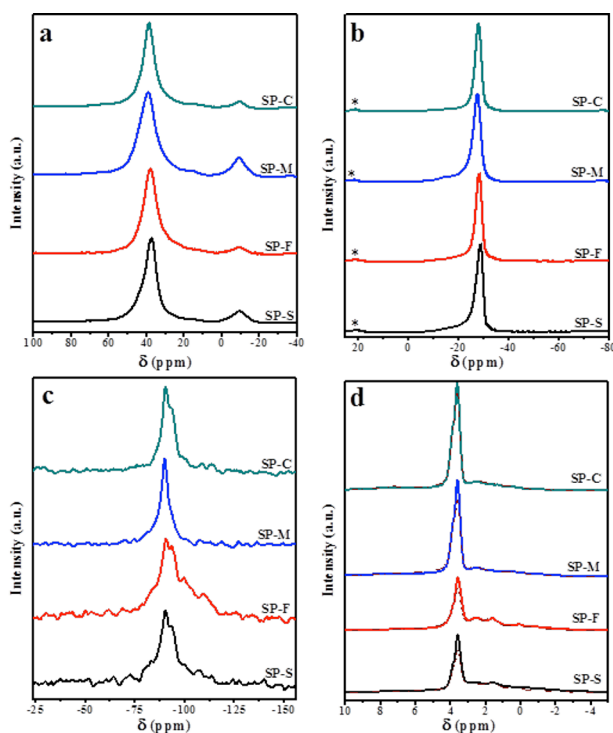


Figure 3. (a) ^{27}Al , (b) ^{31}P , (c) ^{29}Si , and (d) ^1H MAS NMR (solid line) spectra of the calcined SAPO-34 catalysts. In (d), dash dots represent the spectrum of the samples after adsorption of perfluorotributylamine. The asterisk (*) represents the spinning sidebands.

two peaks at 39 and -10 ppm for the four calcined SAPO-34s. The strong peak at low field with chemical shift of 39 ppm arises from tetrahedrally coordinated aluminum atoms.^{28–30} The other one at -10 ppm with low intensity is attributed to the octahedrally coordinated aluminum atoms, formed by the additional coordination of two water molecules to tetrahedrally coordinated framework aluminum atom.²⁸

All the ^{31}P MAS NMR spectra in Figure 3b exhibit the sharp peak at -29 ppm representing the tetrahedrally coordinated phosphorus atom in the coordination state of $(\text{P}(\text{OAl})_4)$.²⁸ The appearance of a very weak and broad peak at -11 ppm suggests the possible existence of a small amount of phosphorus atoms which are additionally coordinated to water molecule to form $(\text{P}(\text{OAl})_4(\text{H}_2\text{O}))$.³¹ The peak at 20 ppm is from spinning sidebands.

Si incorporation into the AlPO framework is of great significance for the generation of acid sites and acid-catalytic properties of SAPO molecular sieves.^{32,33} As indicated in Table 1, the synthesized SAPO-34s with different crystal sizes possess very close Si contents. Their detailed chemical environments of the Si atoms and corresponding acid site formation of these four samples were investigated by ^{29}Si MAS NMR and ^1H MAS NMR.

In the ^{29}Si MAS NMR spectra of SAPO-34s (Figure 3c), six resonance signals appear in the spectra. The signals with chemical shift of -90 and -94 ppm , stemming from the coordination states of $\text{Si}(4\text{Al})$ and $\text{Si}(3\text{Al})$, respectively, show relatively high intensity. The signals at 100 , -108 , and -113 ppm , originated from the coordination states of $\text{Si}(2\text{Al})$, $\text{Si}(1\text{Al})$, and $\text{Si}(0\text{Al})$, respectively, are present in relatively low intensity. In particular, those signals at -108 and -113 ppm in the spectra of SP-M and SP-C are hardly visible. Even in low intensity, for the SAPO-34s with nanoscale crystal size, the signals at -100 , -108 , and -113 ppm are more prominent in intensity than those of medium-sized and coarse SAPO-34s (SP-M and SP-C). It is worthy to note that a signal appears around -85 ppm in the spectra of nanosized SAPO-34s, SP-S, and SP-F. Previous work ascribed it to the silanol group in amorphous aluminosilicates or the breaking of some $\text{Si}-\text{OH}-\text{Al}$ bonds.^{34–36} Considering the high crystallinity of the synthesized SAPO-34s and their rich external surface, we tentatively attribute it to $\text{Si}(\text{OAl})_n(\text{OH})_{4-n}$ from the breaking of some $\text{Si}-\text{OH}-\text{Al}$ bonds, locating in the defect sites or on the outer surface.

It is known that Si atoms incorporate into the AlPO_4 framework by two substitution mechanisms: the first mechanism (SM2) is one Si substitution for one P to form $\text{Si}(4\text{Al})$ entities, which gives rise to negatively charged framework and correspondent one Brønsted acid site. On the other hand, the simultaneous occurrence of two Si incorporation way-SM3 (the double substitution of neighboring Al and P by two Si atoms) would generate multiple chemical environments of Si atom, $\text{Si}(n\text{Al})$ ($n = 3-0$) structures, which leads to the formation of complex acidic bridge hydroxyl groups.³² Usually, the Si coordination states of SAPO molecular sieves depend on the content of Si incorporation or the crystallization condition. For the four samples studied here, which have very close amounts of incorporated Si, the difference in their coordination states (Table 2) is very possibly related to the crystal sizes of the synthesized SAPO-34s resulting from the application of microwave or ordinary heating method. Actually, from the ^{29}Si NMR spectra, in spite of roughly the very similar Si content of these samples, $\text{Si}(n\text{Al})$ ($n = 0-2$) coordination states of the nanosized SAPO-34 samples are more remarkable than that in the medium-sized and coarse SAPO-34s. At the same time, for nanosized samples, the fraction of Si atoms located in $\text{Si}(4\text{Al})$ and $\text{Si}(3\text{Al})$ chemical environment is less than that of SAPO-34s with relatively bigger sizes. The difference in the coordination states of incorporated Si atoms, which is detailed in Table 3, implies that Si incorporation in the nanosized SAPO-34s may generate less acidic bridge hydroxyl groups than the SAPO-34s with larger particle sizes. More Si atoms in the two nanosized SAPO-34s are located in $\text{Si}(\text{OAl})_n(\text{OH})_{4-n}$ as terminal silanols, which implies more external Brønsted acid sites or silanols may exist in them.

The Brønsted acid sites of the SAPO-34s were characterized by means of ^1H MAS NMR spectroscopy. The obtained spectra

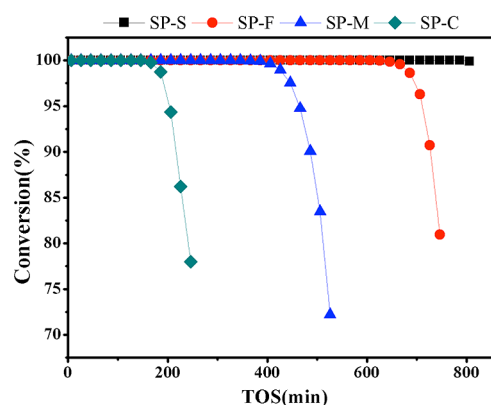
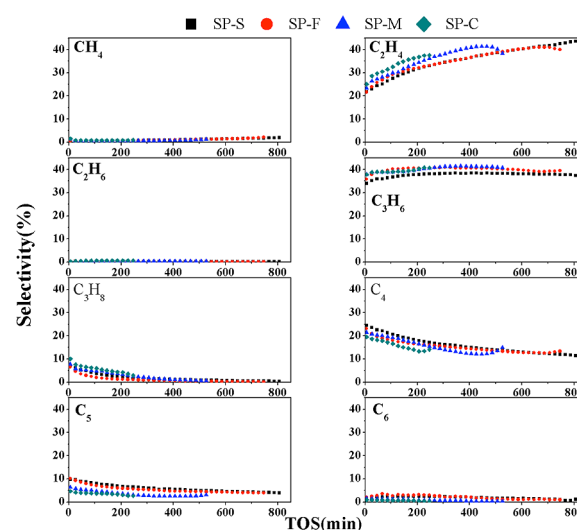
Table 3. ^1H MAS NMR and ^{29}Si MAS NMR Deconvolution Using Gaussian–Lorentzian Function

catalysts		SP-S	SP-F	SP-M	SP-C
^{29}Si MAS NMR	$\text{Si}(\text{OAl})_n(\text{OH})_{4-n}$ (%)	20.0	20.3	13.8	8.5
	Si(4Al) (%)	32.9	22.4	62.5	45.1
	Si(3Al) (%)	23.6	21.0	12.3	27.9
	Si(2Al) (%)	13.4	23.3	5.5	10.8
	Si(1Al) (%)	7.8	1.4	3.5	4.3
	Si(0Al) (%)	2.4	11.7	2.4	3.4
^1H MAS NMR	Si(OH)Al (mmol/g)	0.57	0.56	0.69	0.79
	Si–OH (mmol/g)	0.18	0.20	0.03	0.06
	external B acid sites (%)	26	20	15	7.5

are shown in Figure 3d. Signals at 3.6 ppm are ascribed to bridge hydroxyl groups (Si(OH)Al), indicating the presence of Brønsted acid sites of the synthesized SAPO-34s. Signals at 0–2.4 ppm are assigned to P–OH, Si–OH, and Al–OH groups on the outer crystal surface and framework defects.³⁷ When quantifying the concentration of hydroxyl groups with the signal intensity (see Table 3), it is found that in comparison with the SAPO-34s with ordinary size, silanols (Si–OH at 1.6 ppm) from nanosized catalysts present higher concentration, but bridge hydroxyl groups (Si(OH)Al, at 3.6 ppm) appear with lower concentration, implying relatively low Brønsted acid concentration. This is consistent with the results of ^{29}Si MAS NMR, in which the spectra of SP-S and SP-F show relatively weak signal at –90 ppm compared to SP-M and SP-C, which is attributed to Si(4Al) silicon atoms and responsible for the most effective formation of bridge hydroxyl groups of Si(OH)Al.

Perfluorotributylamine $[(n\text{-C}_4\text{F}_9)_3\text{N}]$ is utilized for quantifying external acidity.³⁸ It is a weak basic molecule with a diameter of 0.94 nm, much larger than the pore size of SAPO-34 crystals. Therefore, when used as a probe molecule in ^1H NMR spectroscopy, perfluorotributylamine can only be adsorbed on the Brønsted acid sites located on the external surface, while those on the internal surface are not accessible for the probe molecule. The intensities of the signal representing the Brønsted acid sites in the ^1H MAS NMR spectra of SAPO-34s before and after perfluorotributylamine adsorption are utilized for quantifying the content of the acid sites located on the external surface. The amounts of external Brønsted acid sites follow the sequence as SP-S > SP-F > SP-M > SP-C (see Table 3), which indicate more acid sites located on the outer surface of the nanosized SAPO-34 than those of the SAPO-34 crystals with ordinary size.

3.3. Catalytic Performance of SAPO-34 Catalysts with Different Crystal Sizes in Methanol Conversion. Catalytic tests of methanol conversion were carried out at 400 °C in a fixed-bed reactor over the four SAPO-34s with different crystal sizes, and the results of conversion and selectivity of the products are given in Figures 4 and 5. The conversion evolution as a function of reaction time shows that at the beginning period of the reaction, the conversion of methanol is 100% for all the four SAPO-34 catalysts, indicating the high initial activity of four samples, but the catalyst lifespan, in which 100% methanol conversion can be kept, and the occurrence of catalyst deactivation vary considerably by the usage of SAPO-34 with different crystal sizes. The methanol conversion over nanoscale SAPO-34s presents very long catalyst lifetime. Over the catalyst of SP-F aggregated by crystals of ca. 20 nm, 100% methanol conversion could be kept for more than 650 min,

**Figure 4.** Methanol conversion variation with time-on-stream over the SAPO-34 catalysts with different crystal particle sizes. Experimental conditions: WHSV = 2 h⁻¹, T = 673 K, catalyst weight = 100 mg.**Figure 5.** Products distribution over the SAPO-34 catalysts with different crystal particle sizes. Experimental conditions: WHSV = 2 h⁻¹, T = 673 K, catalyst weight = 100 mg.

while the deactivation occurs over the catalysts of SP-M and SP-C after time-on-stream of 350 and 150 min. Particularly, the nanosheet-like SP-S with thickness of 20 nm shows the longest catalyst lifetime of 786 min, which is even longer than that of spherical nanocrystal SAPO-34 (SP-F). Our study clearly demonstrates that the stability of nanosized catalysts can be remarkably enhanced compared with the catalysts with bigger sizes, in contrast to the previous work showing that SAPO-34 with the smallest crystallites (<150 nm) deactivated rapidly.^{12d} It is noticed that the lifetime of SP-F aggregated from ca. 20 nm is lower than SP-S nanosheets of 20 nm in thickness. Lifetime is in fact influenced by multiple factors, such as the acidity, porosity, crystal size, and reaction conditions. As indicated in Table 2, SP-S presents more accessible microporous surface than SP-F for methanol conversion, which is also important for the high reactivity and long-term stability of the catalysts. On the other hand, the relatively rich external surface of SP-F compared with SP-S may negatively influence the long-term operation of methanol conversion due to the possible deposition of large coke species on the outer surface. In addition, aggregation of SP-F crystals may also influence the diffusion of reactant and products and thus cause its lower lifetime than SP-S with well-separated nanosheet nanocrystals.

As depicted in Figure 5, for all the four catalysts, light alkenes, such as ethene and propene, are the main products (70–80% in total), indicating that even in different sizes, all the synthesized SAPO-34 catalysts are very selective for the production of light alkenes from methanol. The selectivity of all the generated products varies with time on stream. During the beginning period, the selectivity of ethene and propene is a little low (55–62%) and then increases with prolonging the reaction time. Before the occurrence of the deactivation, the generated light olefins account for about 80% of the hydrocarbon products over the four catalysts. The time course of methanol conversion and product distribution indicate that over SP-C, propane, which is regarded as the byproduct stemming from hydrogen-transfer reaction of olefin products, is more predominantly formed than that over other catalysts.³⁹ At the same time, over SP-F and SP-S, the selectivity of long-chain hydrocarbons of C₄–C₆ products is relatively high. This may result from the olefin methylation-cracking route of special product formation, which usually brings about the hydrocarbon products higher than propene.⁴⁰ The occurrence of methanol conversion via olefins methylation-cracking route is closely related to the structure and acidity of the catalysts, and the acidity concentration is also of great significance in hydrogen-transfer reaction and coke formation. Therefore, the size effect and acid properties over these four catalysts will be considered in the following discussion to give a reasonable explanation of the substantial prolongation of catalyst life with the reduction of crystal size of SAPO-34 catalysts.

After reaction, the SAPO-34 catalysts were discharged and the coke formation over the deactivated catalysts was measured by thermal analysis. As detailed in Table 4, the weight loss from

Table 4. Variation of Coke Formation in Methanol Conversion over SAPO-34s with Different Crystal Particle Sizes

catalysts	SP-S	SP-F	SP-M	SP-C
coke (% g/gcat)	19.81	17.46	19.74	12.98
R_{coke} (mg/min)	0.033	0.036	0.073	0.106
P_{coke} (g/gMeOH)	0.023	0.025	0.050	0.073

the combustion of the retained coke species is 19.81%, 17.46%, 19.74%, and 12.98% for the four SAPO-34 catalysts of SP-S, SP-F, SP-M, and SP-C, respectively. Due to the deactivation occurrence at different time on stream, such as 100% methanol conversion maintained for 786 min for SP-S, 606 min for SP-F, 346 min for SP-M, and 146 min for SP-C, the amount of the coke deposited on the four catalysts corresponds to different duration of methanol conversion. In the present work, to compare the coke formation over the four catalysts with different crystal sizes, the average coking formation rate and the portion of reactant cost on coke generation were also evaluated with the consideration of time on stream and total feeding amount of methanol in the reaction. Coke formation rate (R_{coke}) and the fraction of methanol consumption on coke formation (P_{coke}) in the present work are described as eqs 1 and 2. Methanol feeding is calculated on CH₂ basis. R_{coke} and P_{coke} of the four catalysts are compared in Table 4 together with coke amount from thermal analysis.

$$R_{\text{coke}} \text{ (g/min)} = \text{coke amount (g)/reaction time (min)} \quad (1)$$

$$P_{\text{coke}} \text{ (g/g)} = \text{coke amount (g)/methanol feedstock (g)} \quad (2)$$

Even the coke amount over medium-sized SP-M (19.74%) is close to that over nanosized SP-S and SP-F, and the catalyst with largest size, SP-C, presents the lowest coke amount, their coking rate and the fraction of methanol consumption on coke are much higher than that of SP-S and SP-F. This means very slight coke deposition over nanosized catalysts during methanol conversion, and the cost of methanol feedstock on coke deposition is also lower than those of the catalysts with bigger particle sizes. Slight coke deposition ensures the operation of long-term methanol conversion and makes nanosized SAPO-34s very effective catalysts with high activity and stability for light olefin production.

Besides the difference in lifetime over the four catalysts, continuous coke deposition during methanol conversion also varied the product selectivity. Usually, coke formation and accommodation in the catalyst give rise to the reduction of mass transfer of reactant and products, which causes the reactivity loss of the catalysts and at the same time the generation of smaller products, such as ethene.³⁹ Actually, in our present study, for all the four catalysts, ethene selectivity is improved with time on stream, and the formation of long-chain alkenes, C₄–C₆ alkenes, is depressed due to the diffusion hindrance with coke deposition when prolonging the reaction time. Compared to the bigger size catalysts, SP-C and SP-M, the nanosized catalysts, SP-F and SP-S, present slightly lower ethene selectivity and higher C₄–C₆ products selectivity even though the ethene selectivity increases with time on stream. This indicates the difference of catalyst modification with coke generation. Severe coke deposition over SP-C and SP-M results in the modification of the catalyst and leads to the formation of more ethene products, and less C₄–C₆ products, while slight coke formation over SP-F and SP-S has no remarkable influence on the product diffusion; therefore, relatively high C₄–C₆ products selectivity is presented.

After reactions, the deposited coke species in the deactivated catalysts were analyzed following the method introduced by M. Guisnet.^{25,26} Figure 6 compares the chromatograms of the extracted hydrocarbons from the four deactivated catalysts. Methyl-substituted benzenes (MBs) and methyl-substituted naphthalenes (MNs) appear among the confined organic species for all the four catalysts after deactivation. The formation of polycyclic aromatics, such as phenanthrene and pyrene, varies with the catalyst used. Phenanthrene and pyrene are the most intensified organic species in the chromatogram, implying polycyclic aromatics are predominantly formed as confined coke species over SP-C and SP-M, especially over SP-M. But for nanosized SAPO-34s, SP-F, and SP-S, the intensity of polyaromatics is very low. Notably, over SP-S, even MBs, MNs, and polyaromatics are observed among the confined coke species as the other three SAPO-34 catalysts, and the low intensity of these organic species indicates very slight coke deposition after long-term methanol conversion, which has been confirmed by thermal analysis and coking rate evaluation. Previous studies have proven that methanol conversion over SAPO-34 is based on a hydrocarbon pool mechanism with polymethyl-substituted benzenes as the reaction center and catalyst deactivation is generally accompanied by the progressive formation of methylnaphthalenes and further aging to form the polycyclic aromatic molecules, such as phenanthrene derivatives and pyrene.^{41–43} The accommoda-

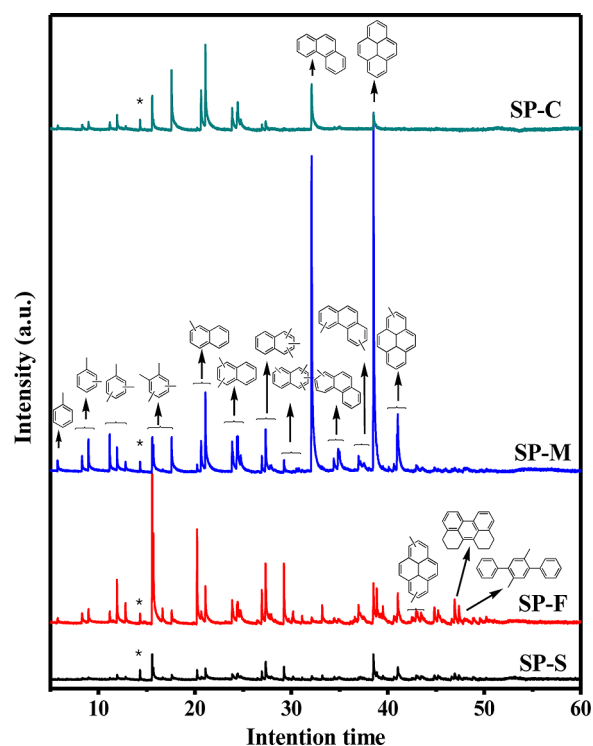


Figure 6. GC-MS chromatograms of occluded organic species retained in the catalysts after methanol conversion at 400 °C. The structures annotated onto the chromatograms are peak identifications in comparison with the mass spectra to those in the NIST database, and the asterisk (*) represents the internal standard (C_2Cl_6).

tion of large polyaromatic species in the nanocages of the catalyst causes the great reduction in mass transfer of reactants and products. Once a significant fraction of the cages of SAPO-34 are occupied by polycyclic aromatics, the deactivation of methanol conversion occurs. The predominant formation of phenanthrene derivatives and pyrene indicates that the deactivation of methanol conversion over SAPO-34 with crystal size of 1 μm (SP-M) and 8 μm (SP-C) should be attributed to mass transfer difficulty caused by the formation polycyclic aromatics in the cage of SAPO-34 catalysts. Over nanosized SP-F and SP-S, the long-term methanol conversion benefits from slight coke deposition or the absence of polycyclic aromatics accommodation in the nanocages. It is worthy to note that some aromatic species appear at retention time of 40–50 min in low intensity, which should be attributed to polycyclic aromatics with more than four fused rings, such as terphenyl derivatives and some other big coke species. These retained compounds are too big to be accommodated in the CHA cage of SAPO-34, so they may form through the conversion of methanol or the secondary reactions of olefins products catalyzed by the external acid sites and locate at the outer surface of the nanosized catalysts, especially over the catalyst of SP-F. The rich external surface and acid sites of SP-S and SP-F have been proved by the measurements of nitrogen adsorption and 1H MAS NMR.

Catalyst deactivation during methanol conversion occurs in a different way. Previous work indicates that acid site coverage or channel blockage resulting from external coke formation is the main reason for the deactivation of ZSM-5 catalyzed MTO reaction.⁴⁴ But when this reaction is performed over SAPO-34 with cage structure, huge coke deposition and accommodation

in the CHA cage will cause the enhanced diffusion restriction, and therefore internal coke formation is the main reason for deactivation. As the main coke species of SAPO-34, polycyclic aromatics were suggested to be generated from the aging of polymethyl-substituted benzenes and methylnaphthalenes with the hydrogen transfer reaction between primary olefins and these hydrocarbon pool species.⁴⁵ On the other hand, propene and other light olefins, as the main products of MTO, are also highly reactive in acid catalysis.⁴⁶ On acid catalyst, these molecules may also possibly undergo oligomerization and hydrogen transfer to form the aromatic coke molecules.^{25,39} Therefore, deactivation is closely related to side reactions, such as hydrogen transfer. Hydrogen transfer index (HTI, C_3H_8/C_3H_6) was employed in the present study to evaluate the hydrogen transfer level of secondary transformation of olefins products. Figure 7 compares the HTI value of steady-state

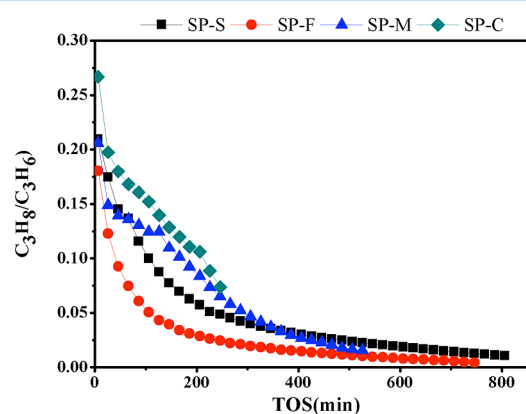


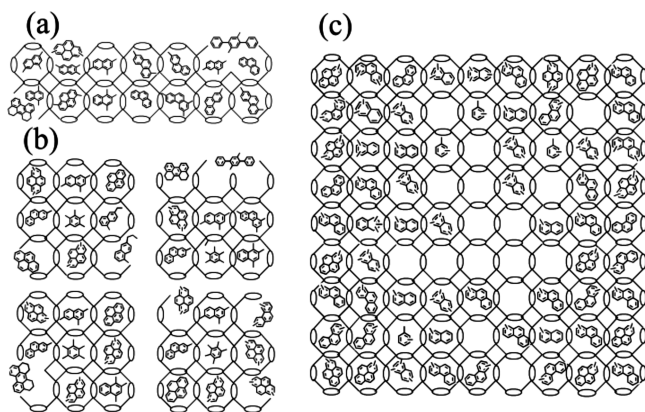
Figure 7. Hydrogen transfer index (HTI, C_3H_8/C_3H_6) value of methanol conversion over SAPO-34 catalysts.

MTO reactions over the four SAPO-34s with different crystal sizes. Low HTI level over SP-S and SP-F corresponds to the low coking rate, indicating that the reduction of crystal size of the SAPO-34 catalyst depresses the polycyclic aromatics formation from the reduction of reaction between the olefin products and the confined methylbenzenes and methylnaphthalenes. In this way, coke formation over SP-F and SP-S is eliminated, and the catalyst life can be prolonged remarkably.

In the 1H MAS NMR measurement, the four SAPO-34 catalysts present different Brønsted acid concentrations. Roughly more bridge hydroxyl groups appear on SP-M and SP-C than those over nanosized catalysts of SP-S and SP-F. The bimolecular reaction, such as hydrogen transfer, is depressed over the catalysts with low Brønsted acid concentration. But in the present work, it is worthy to note that the silicon content is very close for the four catalysts and the slight reduction of acid sites over SP-F and SP-S cannot satisfyingly explain the extremely long catalyst life presented over the two nanosized catalysts. The size effect may play a more important role in varying the performance over the four catalysts. The enhancement of mass transfer of reactant and products of methanol conversion and the improved exposure of catalyst surface to the reactant ensure the high reactivity and long-term stability of nanosized SAPO-34s.

A compressed, two-dimensional view of catalyst particle with confined organics in the CHA cage of SAPO-34 is depicted in Scheme 1 to demonstrate the location of retained coke species

Scheme 1. Coke Location and Deactivation Mode of SAPO-34 Catalysts: (a) SP-S, (b) SP-F, and (c) SP-M and SP-C



after methanol conversion. The four SAPO-34 catalysts vary with crystal sizes, and their deactivation also occurs in different ways. As indicated in the confined organic analysis of the deactivated catalysts of SP-M and SP-C with GC-MS, the formation and accommodation of big aromatic products block the diffusion path of methanol and cause mass transfer difficulty in accessing the active reaction center of methanol conversion. When deactivation occurs, due to the entrance blockage of the catalyst particles, some reactive CHA cages in the central part of SAPO-34 crystal particles leave no contact with the reactant during methanol conversion. Consequently, low catalytic efficiency presents in the reaction over SP-M and SP-C accompanied by the quick deactivation and short catalyst lifetime. For the nanosized crystal particles of SAPO-34s, SP-S, and SP-F, small size and rich outer surface give rise to remarkably enhanced mass transfer of reactant and generated products. Most of the reactive centers in the cage are accessible during the methanol conversion, and the usage of these nanosized catalysts is very efficient. At the same time, quick leaving of products, such as the active olefin products, also reduces the occurrence of hydrogen-transfer reaction between olefin products and confined aromatics, and the formation of hydrogen-unsaturated products, such as polycyclic aromatics which cause deactivation, are also depressed. SP-S presents the shortest diffusion length at the vertical direction for methanol and generated olefins, so the longest catalyst life and highest reaction stability are observed over this sheetlike nanosized SAPO-34. Some polycyclic aromatics with bigger size than pyrene are observed over the nanosized SAPO-34s after reaction, which may stem from the coke species deposited on the rich external surface of nanosized catalysts.

4. CONCLUSION

Four highly crystalline SAPO-34 molecular sieves with different crystallite sizes varying from 20 nm to 8 μm were synthesized from the gel with the same composition using TEOH as the structure directing agent. Catalytic test of MTO reactions over these SAPO-34s demonstrates that the catalyst deactivation and the catalyst lifetime are strongly dependent on the crystallite sizes. The nanosized SAPO-34 catalysts exhibit longer lifetime in the methanol conversion reactions compared with those with ordinary crystallite size. Particularly, the nanosheet-like SAPO-34 with thickness of 20 nm gives rise to remarkably enhanced lifetime. The evaluation of coking rate and the fraction of methanol consumption on coke indicate very slight coke

deposition over nanosized SAPO-34s during methanol conversion, which ensures the operation of long-term methanol conversion. It is believed that the enhancement of mass transfer of reactant and generated products during methanol conversion as well as the improved exposure of catalyst surface to the reactant contribute to the remarkably enhanced lifetime of nanosized SAPO-34 catalysts.

■ ASSOCIATED CONTENT

Supporting Information

TEM image of SP-F; N_2 adsorption–desorption isotherms of four synthesized SAPO-34s. This material is available free of charge via the Internet at <http://pubs.acs.org>.

■ AUTHOR INFORMATION

Corresponding Author

*E-mail jihong@jlu.edu.cn; tel. 0086-431-8516-8608; fax 0086-431-8516-8608 (J.Y.). E-mail liuzm@dicp.ac.cn; tel. 0086-411-84379335; fax 0086-411-84379335 (Z.L.).

Notes

The authors declare no competing financial interest.

■ ACKNOWLEDGMENTS

We thank the National Natural Science Foundation of China (No. 21273230, 21273005, and 21103180) and the National Basic Research Program of China (grant 2011CB808703) for financial support of this work.

■ REFERENCES

- (1) Chang, C. D. Hydrocarbons from Methanol. *Catal. Rev.* **1983**, *25*, 1–118.
- (2) Chang, C. D. Methanol Conversion to Light Olefins. *Catal. Rev.* **1984**, *26*, 323–345.
- (3) Chang, C. D.; Silvestri, A. J. The Conversion of Methanol and Other O-Compounds to Hydrocarbons over Zeolite Catalysts. *J. Catal.* **1977**, *47*, 249–259.
- (4) Keil, F. J.; Hinderer, J.; Garayhi, A. R. Diffusion and Reaction in ZSM-5 and Composite Catalysts for the Methanol-to-Olefins Process. *Catal. Today* **1999**, *50*, 637–650.
- (5) Stocker, M. Methanol-to-Hydrocarbons: Catalytic Materials and Their Behavior. *Microporous Mesoporous Mater.* **1999**, *29*, 3–48.
- (6) Gayubo, A. G.; Aguayo, A. T.; Olazar, M.; Vivanco, R.; Bilbao, J. Kinetics of the Irreversible Deactivation of the HZSM-5 Catalyst in the MTO Process. *Chem. Eng. Sci.* **2003**, *58*, S239–S249.
- (7) Marchi, A. J.; Froment, G. F. Catalytic Conversion of Methanol to Light Alkenes on SAPO Molecular Sieves. *Appl. Catal.* **1991**, *71*, 139–152.
- (8) Liang, J.; Li, H. Y.; Zhao, S.; Guo, W. G.; Wang, R. H.; Ying, M. L. Characteristics and Performance of SAPO-34 Catalyst for Methanol to Olefin Conversion. *Appl. Catal.* **1990**, *64*, 31–40.
- (9) Keil, F. J. Methanol-to-Hydrocarbons: Process Technology. *Microporous Mesoporous Mater.* **1999**, *29*, 49–66.
- (10) Inui, T.; Phatanasri, S.; Matsuda, H. Highly Selective Synthesis of Ethene from Methanol on a Novel Nickel-Silicoaluminophosphate Catalyst. *J. Chem. Soc., Chem. Commun.* **1990**, 205–206.
- (11) Socha, R. F.; Chang, C. D.; Gould, R. M.; Kane, S. E.; Avidan, A. A. Fluid-Bed Studies of Olefin Production from Methanol. *ACS Symp. Ser.* **1987**, *328*, 34–41.
- (12) Vora, B. V.; Marker, T. L.; Barger, P. T.; Nielsen, H. R.; Kvisle, S.; Fuglerud, T. Economic Route for Natural Gas Conversion to Ethylene and Propylene. *Stud. Surf. Sci. Catal.* **1997**, *107*, 87–98.
- (13) Barger, P. T. Methanol Conversion Process Using SAPO Catalysts. U.S. Patent 5,095,163, 1992.
- (14) Larsen, S. C. Nanocrystalline Zeolites and Zeolite Structures: Synthesis, Characterization, and Applications. *J. Phys. Chem. C* **2007**, *111*, 18464–18474.

- (15) Tago, T.; Konno, H.; Nakasaka, Y.; Masuda, T. Size-Controlled Synthesis of Nano-Zeolites and Their Application to Light Olefin Synthesis. *Catal. Surv. Asia* **2012**, *16*, 148–163.
- (16) Chen, D.; Moljord, K.; Fuglerud, T.; Holmen, A. The Effect of Crystal Size of SAPO-34 on the Selectivity and Deactivation of the MTO Reaction. *Microporous Mesoporous Mater.* **1999**, *29*, 191–203.
- (17) Chen, D.; Moljord, K.; Holmen, A. A Methanol to Olefins Review: Diffusion, Coke Formation, and Deactivation SAPO Type Catalysts. *Microporous Mesoporous Mater.* **2012**, *164*, 239–250.
- (18) Razavian, M.; Halladj, R.; Askari, S. Recent Advances in Silicoaluminophosphate Nanocatalysts Synthesis Techniques and Their Effects on Particle Size Distribution. *Rev. Adv. Mater. Sci.* **2011**, *29*, 83–99.
- (19) Nishiyama, N.; Kawaguchi, M.; Hirota, Y.; Van Vu, D.; Egashira, Y.; Ueyama, K. Size Control of SAPO-34 Crystals and Their Catalyst Lifetime in the Methanol-to-Olefin Reaction. *Appl. Catal., A* **2009**, *362*, 193–199.
- (20) Lee, K. Y.; Chae, H. J.; Jeong, S. Y.; Seo, G. Effect of Crystallite Size of SAPO-34 Catalysts on Their Induction Period and Deactivation in Methanol-to-Olefin Reactions. *Appl. Catal., A* **2009**, *369*, 60–66.
- (21) Hirota, Y.; Murata, K.; Miyamoto, M.; Egashira, Y.; Nishiyama, N. Light Olefins Synthesis from Methanol and Dimethylether over SAPO-34 Nanocrystals. *Catal. Lett.* **2010**, *140*, 22–26.
- (22) Askari, S.; Halladj, R.; Sohrabi, M. Methanol Conversion to Light Olefins over Sonochemically Prepared SAPO-34 Nanocatalyst. *Microporous Mesoporous Mater.* **2012**, *163*, 334–342.
- (23) Jang, H. G.; Min, H. K.; Lee, J. K.; Hong, S. B.; Seo, G. SAPO-34 and ZSM-5 Nanocrystals' Size Effects on their Catalysis of Methanol-to-Olefin Reactions. *Appl. Catal., A* **2012**, *437*, 120–130.
- (24) Lin, S.; Li, J.; Sharma, R. P.; Yu, J.; Xu, R. Fabrication of SAPO-34 Crystals with Different Morphologies by Microwave Heating. *Top. Catal.* **2010**, *53*, 1304–1310.
- (25) Guisnet, M.; Magnoux, P. Organic Chemistry of Coke Formation. *Appl. Catal., A* **2001**, *212*, 83–96.
- (26) Guisnet, M. "Coke" Molecules Trapped in the Micropores of Zeolites as Active Species in Hydrocarbon Transformations. *J. Mol. Catal. A: Chem.* **2002**, *182*, 367–382.
- (27) Vomscheid, R.; Briend, M.; Peltre, M. J.; Man, P. P.; Barthomeuf, D. The Role of the Template in Directing the Si Distribution in SAPO Zeolites. *J. Phys. Chem.* **1994**, *98*, 9614–9618.
- (28) Blackwell, C. S.; Patton, R. L. Aluminum-27 and Phosphorus-31 Nuclear Magnetic Resonance Studies of Aluminophosphate Molecular Sieves. *J. Phys. Chem.* **1984**, *88*, 6135–6139.
- (29) Prakash, A. M.; Unnikrishnan, S. Synthesis of SAPO-34: High Silicon Incorporation in the Presence of Morpholine as Template. *J. Chem. Soc., Faraday Trans.* **1994**, *90*, 2291–2296.
- (30) Ashtekar, S.; Chilukuri, S. V. V.; Chakrabarty, D. K. Small-Pore Molecular Sieves SAPO-34 and SAPO-44 with Chabazite Structure: A Study of Silicon Incorporation. *J. Phys. Chem.* **1994**, *98*, 4878–4883.
- (31) Yan, Z. M.; Chen, B. H.; Huang, Y. A Solid-State NMR Study of the Formation of Molecular Sieve SAPO-34. *Solid State Nucl. Magn. Reson.* **2009**, *35*, 49–60.
- (32) Sastre, G.; Lewis, D. W.; Catlow, C. R. A. Modeling of Silicon Substitution in SAPO-5 and SAPO-34 Molecular Sieves. *J. Phys. Chem. B* **1997**, *101*, 5249–5262.
- (33) Tan, J.; Liu, Z. M.; Bao, X. H.; Liu, X. C.; Han, X. W.; He, C. Q.; Zhai, R. S. Crystallization and Si Incorporation Mechanisms of SAPO-34. *Microporous Mesoporous Mater.* **2002**, *53*, 97–108.
- (34) Doremieuxmorin, C.; Martin, C.; Bregeault, J. M.; Fraissard, J. Multinuclear High-Resolution Solid-State Nuclear Magnetic Resonance Studies of Amorphous Silica-Aluminas. *Appl. Catal.* **1991**, *77*, 149–161.
- (35) Zhang, L.; Bates, J.; Chen, D. H.; Nie, H. Y.; Huang, Y. N. Investigations of Formation of Molecular Sieve SAPO-34. *J. Phys. Chem. C* **2011**, *115*, 22309–22319.
- (36) Briend, M.; Vomscheid, R.; Peltre, M. J.; Man, P. P.; Barthomeuf, D. Influence of the Choice of the Template on the Short- and Long-Term Stability of SAPO-34 Zeolite. *J. Phys. Chem.* **1995**, *99*, 8270–8276.
- (37) Hunger, M. Bronsted Acid Sites in Zeolites Characterized by Multinuclear Solid-State NMR Spectroscopy. *Catal. Rev.* **1997**, *39*, 345–393.
- (38) Zhang, W. P.; Ma, D.; Liu, X. C.; Liu, X. M.; Bao, X. H. Perfluorotributylamine as a Probe Molecule for Distinguishing Internal and External Acidic Sites in Zeolites by High-Resolution H-1 MAS NMR Spectroscopy. *Chem. Commun.* **1999**, 1091–1092.
- (39) Hereijgers, B. P. C.; Bleken, F.; Nilsen, M. H.; Svelle, S.; Lillerud, K. P.; Bjorgen, M.; Weckhuysen, B. M.; Olsbye, U. Product Shape Selectivity Dominates the Methanol-to-Olefins (MTO) Reaction over H-SAPO-34 Catalysts. *J. Catal.* **2009**, *264*, 77–87.
- (40) Li, J. Z.; Wei, Y. X.; Liu, G. Y.; Qi, Y.; Tian, P.; Li, B.; He, Y. L.; Liu, Z. M. Comparative Study of MTO Conversion over SAPO-34, H-ZSM-5 and H-ZSM-22: Correlating Catalytic Performance and Reaction Mechanism to Zeolite Topology. *Catal. Today* **2011**, *171*, 221–228.
- (41) Dahl, I. M.; Kolboe, S. On the Reaction-Mechanism for Hydrocarbon Formation from Methanol over SAPO-34. 1. Isotopic Labeling Studies of the Co-Reaction of Ethene and Methanol. *J. Catal.* **1994**, *149*, 458–464.
- (42) Dahl, I. M.; Kolboe, S. On the Reaction-Mechanism for Hydrocarbon Formation from Methanol over SAPO-34. 2. Isotopic Labeling Studies of the Co-Reaction of Propene and Methanol. *J. Catal.* **1996**, *161*, 304–309.
- (43) Haw, J. F.; Song, W. G.; Marcus, D. M.; Nicholas, J. B. The Mechanism of Methanol to Hydrocarbon Catalysis. *Acc. Chem. Res.* **2003**, *36*, 317–326.
- (44) Schulz, H. "Coking" of Zeolites during Methanol Conversion: Basic Reactions of the MTO-, MTP-, and MTG Processes. *Catal. Today* **2010**, *154*, 183–194.
- (45) Bjorgen, M.; Olsbye, U.; Kolboe, S. Coke Precursor Formation and Zeolite Deactivation: Mechanistic Insights from Hexamethylbenzene Conversion. *J. Catal.* **2003**, *215*, 30–44.
- (46) Espinoza, R. L. Oligomerization vs Methylation of Propene in the Conversion of Dimethyl Ether (or Methanol) to Hydrocarbons. *Ind. Eng. Chem. Prod. Res. Dev.* **1984**, *23*, 449–452.